Energy Flow Dynamics within Cofacial and Slip-Stacked Perylene-3,4-dicarboximide Dimer Models of π-Aggregates

Rebecca J. Lindquist,[†] Kelly M. Lefler,[†] Kristen E. Brown, Scott M. Dyar, Eric A. Margulies, Ryan M. Young, and Michael R. Wasielewski*

Department of Chemistry and Argonne−Northwestern Solar Energy Research (ANSER) Center, Northwestern University, Evanston, Illinois 60208-3113, United States

S *Supporting Information*

ABSTRACT: Robust perylene-3,4-dicarboximide (PMI) π-aggregates provide important light-harvesting and electron−hole pair generation advantages in organic photovoltaics and related applications, but relatively few studies have focused on the electronic interactions between PMI chromophores. In contrast, structure−function relationships based on π−π stacking in the related perylene-3,4:9,10-bis(dicarboximides) (PDIs) have been widely investigated. The performance of both PMI and PDI derivatives in organic devices may be limited by the formation of low-energy excimer trap states in morphologies where interchromophore coupling is strong. Here, five covalently bound PMI dimers with varying degrees of electronic interaction were studied to probe the relative chromophore orientations that lead to excimer energy trap states. Femtosecond near-infrared transient absorption spectroscopy was used to observe the growth of a low-energy transition at ∼1450−1520 nm characteristic of the excimer state in these covalent dimers. The excimer-state absorption appears in ∼1 ps, followed by conformational relaxation over 8−17 ps. The excimer state then decays in 6.9−12.8 ns, as measured by time-resolved fluorescence spectroscopy. The excimer lifetimes reach a maximum for a slip-stacked geometry in which the two PMI molecules are displaced along their long axes by one phenyl group (∼4.3 Å). Additional displacement of the PMIs by a biphenyl spacer along the long axis prevents excimer formation. Symmetry-breaking charge transfer is not observed in any of the PMI dimers, and only a small triplet yield (<5%) is observed for the cofacial PMI dimers. These data provide structural insights for minimizing excimer trap states in organic devices based on PMI derivatives.
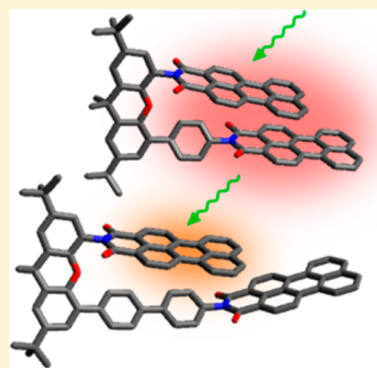
INTRODUCTION

The rational design of materials that incorporate self-assembly of small-molecule building blocks for organic electronic and photovoltaic applications necessitates an understanding of the changes in optical and electronic behavior that result from the relative orientations of chromophores.[1−7] Strong electronic coupling between chromophores can result in undesirable formation of low-energy excimer trap states that inhibit more desirable exciton diffusion,[1,8,9] charge transfer and transport,[10,11] and singlet exciton fission.[12−14]

Perylene-3,4-dicarboximides (PMIs) are of particular interest for self-assembled organic electronics and photovoltaics because of their strong absorptivity in the midvisible spectral region, high excited-state energies, and thermal and photochemical stability.[15−19] The relatively mild redox potentials of PMI (E_{OX} = 1.41 V vs SCE and E_{RED} = −1.00 V vs SCE) make it an attractive candidate as either an electron donor or electron acceptor.[20] PMI also offers interesting self-assembly opportunities because of the 6.4 D permanent ground-state dipole moment directed along the long axis of the molecule,[21] which could enhance the bulk dipolar nature of an aligned nanostructure.

PMI has been incorporated into several donor−acceptor systems for energy and electron transfer studies,[22−37] but relatively few studies have focused on the electronic interactions between PMI chromophores in either covalent or self-assembled systems.[21,38−40] In contrast, the well-known aggregation of the related family of perylene-3,4:9,10-bis-(dicarboximides) (PDIs) based on π−π stacking of the perylene core[4,5,41−58] has inspired detailed investigations of structure−function relationships in a variety of simple covalent and intermolecular PDI aggregates.[41,42,59−71] Among these systems, dimer models provide particularly helpful fundamental understanding of energy and electron transfer processes. Importantly, excimer states have been observed for PDI cyclophanes[70,72] and H- and J-type dimers with xanthene (Xan)[59−61] and triptycene scaffolds.[71]

Here we report the synthesis and photophysics of a series of five covalent cofacial and slip-stacked PMI dimers bridged by a Xan scaffold (Figure 1). In molecules **1−3**, the method of attachment to the Xan bridge is varied to create different degrees of displacement of the PMI π system along the short molecular axis. In molecule **3**, an additional small displacement along the long axis is introduced by placing the two PMIs with their dipole moments in opposite directions. In molecules **4**
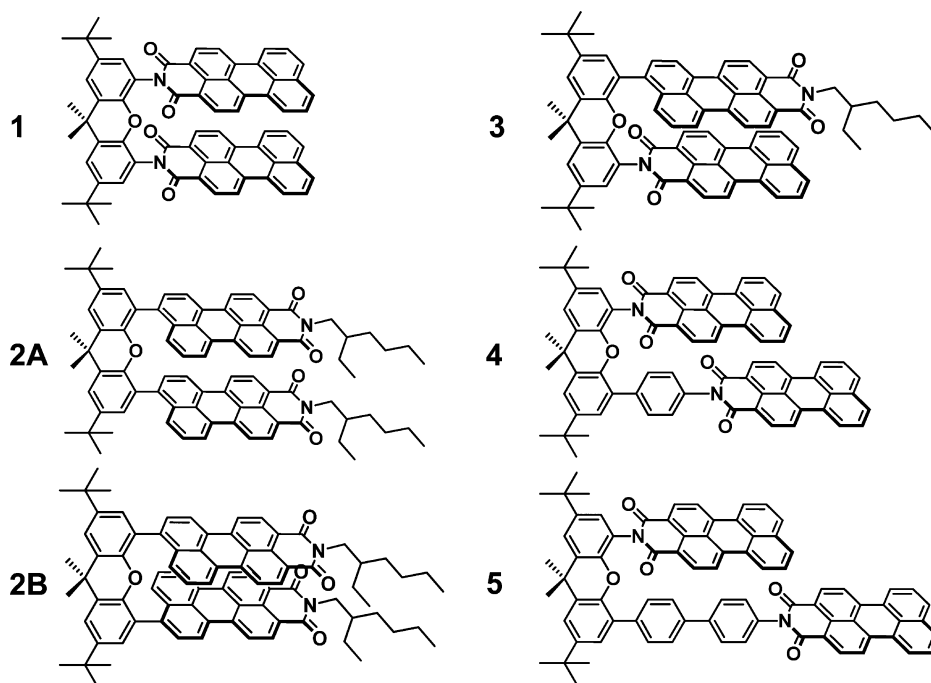
Figure 1. Structures of **1−5**. Both isomers of **2** are shown.

Scheme 1. Synthesis of Precursor Compounds and 1[a]
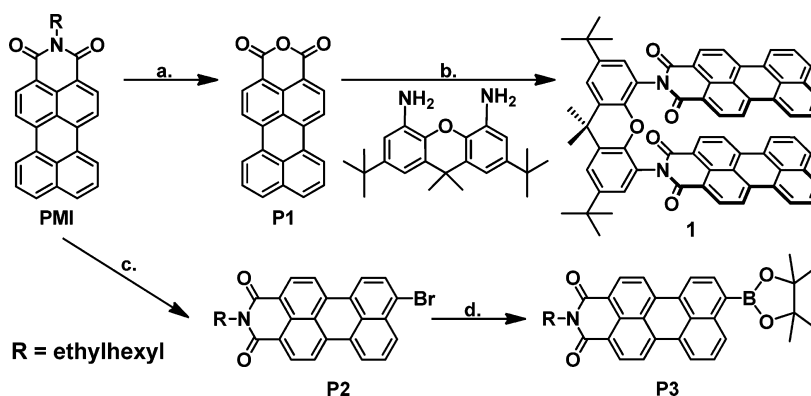
[a]Reaction conditions: (a) (1) KOH, *t*-BuOH, reflux, 2.5 h; (2) AcOH, RT, 30 min, 55%. (b) 2,7-Di-*tert*-butyl-9,9-dimethyl-4,5-diaminoxanthene, pyridine, imidazole, reflux, 2 days, 52%. (c) Br₂, CH₂Cl₂, reflux, 2 h, 93%. (d) Bis(pinacolato)diboron, KOAc, Pd(dppf)Cl₂·CH₂Cl₂, dioxane, 85 °C, 16 h, 81%.

and **5**, phenyl and biphenyl spacers, respectively, are used to further vary the π overlap along the long molecular axis. When the PMIs are connected to the Xan bridge through the perylene core, a 2-ethylhexyl group is attached to the imide nitrogen atom to increase the solubility and minimize disruption of the $\pi-\pi$ stacking interactions. We investigate the nature of the excimer states in the PMI dimers and make comparisons with the energetics and dynamics of the analogous state in PDI dimers using the red-shifted fluorescence emission and the transient near-infrared (NIR) excimer absorption band similar to those previously observed for PDI excimers[70,71] and other aromatic aggregates.[73]

■ EXPERIMENTAL SECTION

Materials and Synthesis. The syntheses of **1−5** are depicted in Schemes 1 and 2 and described explicitly in the Supporting Information (SI). Reagents and spectrophotometric-grade solvents were purchased from Sigma-Aldrich and used without further purification except where noted. Dichloromethane for all of the spectroscopy experiments was dried using a Glass Contour solvent system. Intermediates and final products were characterized with ¹H and ¹³C NMR spectroscopy and high-resolution mass spectrometry (see the SI). ¹³C NMR spectra could not be obtained for molecules **4** and **5** because of their poor solubility. Compounds **1−5** and **PMI** were further purified by HPLC for steady-state and time-resolved fluorescence measurements.

X-ray Crystallography. Crystals of dimers **1** and **5** were grown by slow diffusion of methanol vapor into a chloroform solution of the compounds. The crystals were mounted on polymer loops with Paratone oil, and the data were collected at 100 K on a Bruker Kappa APEX II CCD diffractometer equipped with a Cu Kα IμS microfocus source with MX optics and a Bruker Kappa APEX II CCD diffractometer equipped with a Cu Kα IμS microfocus source with Quazar optics, respectively. The data for dimer **1** were processed and absorption-corrected using TWINABS, and the data for dimer **5** were absorption-corrected with SADABS. The structures were solved with SHELXT and refined with SHELXL using Olex2 software.

Scheme 2. Synthesis of 2–5[a]
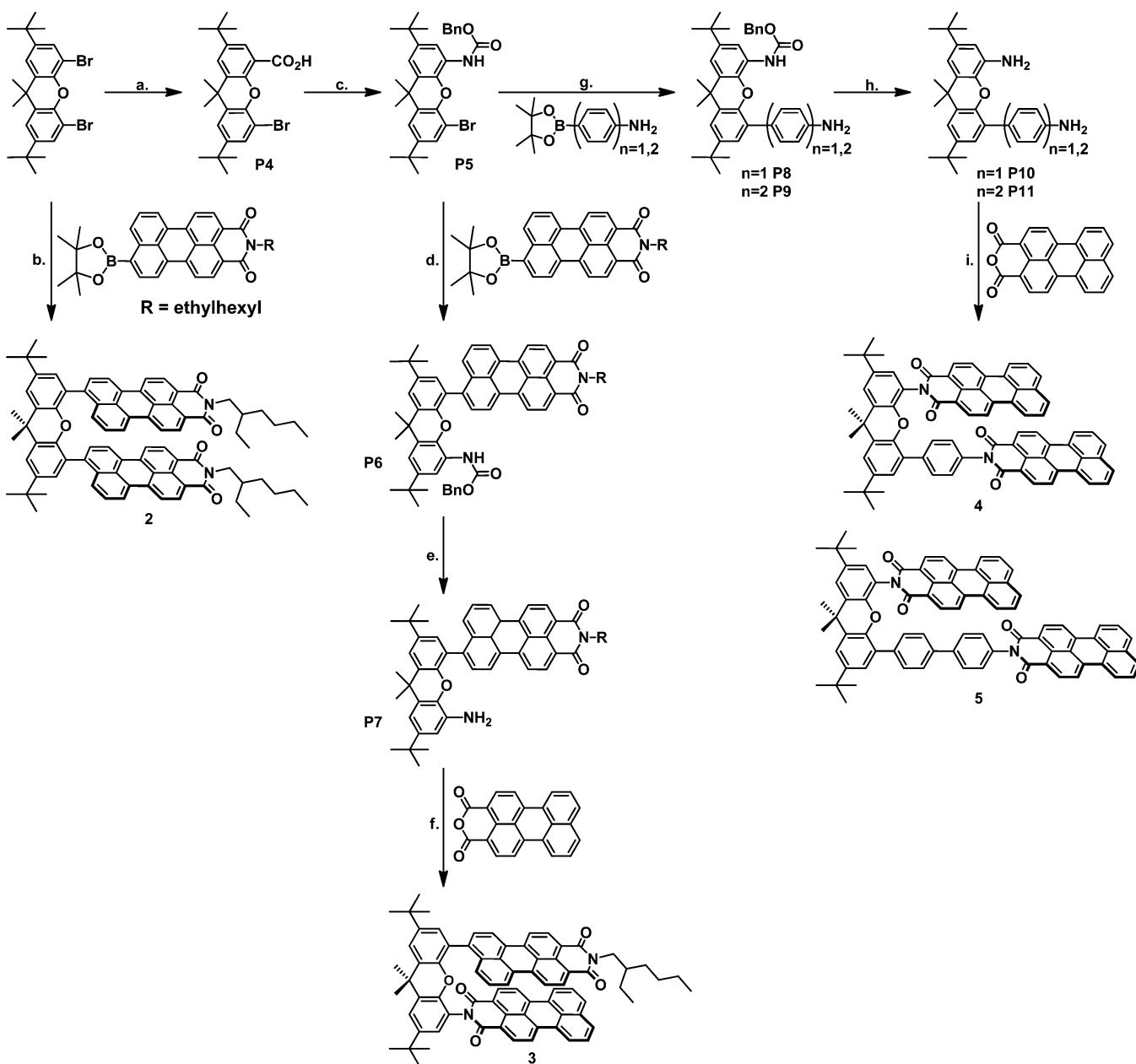
[a]Reaction conditions: (a) (1) n-BuLi (1.6 M in hexanes), THF, −78 °C, 1 h; (2) CO₂(g), −78 °C, 1 h, warmed to RT, 75%. (b) **P3**, Na₂CO₃, Pd(PPh₃)₄, toluene, EtOH, H₂O, 80 °C, 16 h, 33%. (c) (1) Diphenylphosphoryl azide, triethylamine, toluene, 15 min, 22 °C; (2) benzyl alcohol, 80 °C, 14 h, 97%. (d) **P3**, Na₂CO₃, Pd(PPh₃)₄, toluene, EtOH, H₂O, 80 °C, 16 h, 48%. (e) Pd/C (10%), H₂, EtOAc, RT, 3 h, 96%. (f) **P1**, imidazole, 140 °C, 1 day, 38%. (g) 4-Aminophenyl boronic acid pinacol ester (**4**) or 4-aminobiphenyl boronic acid pinacol ester (**5**), K₂CO₃, Pd(PPh₃)₄· toluene, EtOH, H₂O, 85 °C, 17 h, 67% (**4**), 78% (**5**). (h) Pd/C (10%), EtOH, EtOAc, H₂ atmosphere, 22 °C, 3 h, quantitative. (i) **P1**, imidazole, 140 °C, 1 day, 31% (**4**), 33% (**5**).

Steady-State Optical Spectroscopy. Steady-state absorption spectra were collected at room temperature in a 1 mm cuvette in CH₂Cl₂ (optical density 0.3−0.7 at the maximum) using a Shimadzu 1800 spectrometer. Fluorescence measurements were made on a PTI Quanta-Master 1 single-photon-counting fluorimeter in a right-angle configuration with a 10 mm quartz cuvette. Quantum yield measurements in CH₂Cl₂ (optical density 0.01−0.05 at the maximum) used N-(2,6-diisopropylphenyl)perylene-3,4-dicarboximide in toluene as a standard.[74]

Time-Resolved Optical Spectroscopy. Picosecond time-resolved fluorescence (TRF) measurements were made using a laboratory-built cavity-dumped Ti:sapphire laser system with a streak camera (Hamamatsu C4780 Streakscope) as previously described.[14,75]

Samples were prepared in 1 mm quartz cuvettes in dichloromethane with optical densities of 0.1 at the excitation wavelength (416 nm). All data were acquired in single-photon-counting mode using the Hamamatsu HPD-TA software. The temporal resolution was approximately 2% of the sweep window.

Femtosecond vis−NIR transient absorption (fsTA) experiments were conducted using a regeneratively amplified Ti:sapphire laser system as previously described.[76] Samples in dichloromethane were irradiated at 490 nm in 2 mm glass cuvettes with 110 fs, 0.2−0.5 μJ pulses focused to a 100 μm diameter spot. The optical density at the excitation wavelength was maintained at 0.5−0.7. Transient spectra were acquired for 5 s per pump−probe time delay point. The temporal resolution was ∼120−280 fs.

Nanosecond transient absorption (nsTA) experiments were performed by exciting samples in dichloromethane with 7 ns, 1.5 mJ, 532 nm pulses from the output of an optical parametric oscillator (Continuum Panther) pumped by the frequency-tripled output of a Nd:YAG laser (Continuum Precision II 8000). The probe was generated by a pulsed xenon flashlamp (EG&G Electro-Optics FX-200). Kinetic traces were collected from 390 to 800 nm at 5 nm intervals, omitting 520−540 nm. Spectra were constructed by merging the kinetic traces (binned to 3 ns steps, 100 laser shots per kinetic trace). Samples were prepared with optical densities of 0.5−0.7 and were degassed with three freeze−pump−thaw cycles prior to irradiation in 10 mm quartz cuvettes.

All of the fsTA data were corrected for group delay dispersion (GDD, or "chirp") and t_0 prior to kinetic analysis. The three-dimensional data sets from TRF (fluorescence counts vs time and wavelength) were analyzed by singular value decomposition (SVD) and global fitting to obtain the kinetic time constants and their decay-associated spectra (DAS) using Surface Xplorer software, version 2.2.3 (Ultrafast Systems LLC, Sarasota, FL).[77] These time constants, which are too long to be accurately measured on the fsTA apparatus, were input as the longest lifetimes and held constant when fitting the combined visible and NIR fsTA data according to the same SVD and global fitting procedure. The long-lived broad NIR features that resulted from this treatment were fit to Gaussian functions for comparison between dimers.

Computational Methods. The ground-state geometries of **1−5** were initially relaxed using molecular mechanics with the MMFF294 force field as implemented in the Avogadro 1.1.0 software.[78] Starting from this geometry, singlet ground-state structures were subsequently relaxed using density functional theory (DFT) with Grimme's D-3 dispersion correction[79] as implemented in the QChem 4.0 software.[80] All of the DFT calculations made use of the B3LYP exchange−correlation functional with a split-valence double-ζ basis set with added polarization functions (6-31G*). Implicit solvation was implemented using a polarizable continuum model (CPCM/SWIG) with 110 grid points on all atoms. A dielectric constant of 8.93 (dichloromethane) was used in all cases. Images of the optimized structures were generated with PyMol 1.2r1.[81] The 2-ethylhexyl groups of molecules **2** and **3** were replaced with methyl groups to save computation time.

RESULTS

Synthesis and Structure. Syntheses of **PMI**,[82] compounds **P4** and **P5**,[83] and compounds **P8−P11**[69] have been reported previously. Precursors **P1−P3** and molecule **1** were synthesized according to literature procedures, as shown in Scheme 1. **PMI** was hydrolyzed with KOH in *tert*-butyl alcohol to afford compound **P1**.[15] **PMI** was selectively brominated at the 9-position with bromine in refluxing dichloromethane[84] and then converted to the boronic ester, compound **P3**, using bis-(pinacolato)diboron with potassium acetate and [1,1′-bis-(diphenylphosphino)ferrocene]dichloropalladium(II)·dichloromethane complex in dioxane.[85] Molecule **1** was synthesized using an imide condensation of **P1** and 2,7-di-*tert*-butyl-9,9-dimethyl-4,5-diaminoxanthene.[15]

The syntheses of molecules **2−5** are shown in Scheme 2. Molecule **2** was synthesized by a Suzuki−Miyaura cross-coupling reaction between **P3** and 2,7-di-*tert*-butyl-9,9-dimethyl-4,5-dibromoxanthene using sodium carbonate and tetrakis(triphenylphosphine)palladium(0) in a toluene/ethanol/water solution.[86] The asymmetrical Xan spacers for **3−5** were synthesized according to conditions published by Malaisé and co-workers to give **P4** and **P5**.[83] A Suzuki−Miyaura cross-coupling reaction of **P5** with **P3** using sodium carbonate and tetrakis(triphenylphosphine)palladium(0) in a toluene/ethanol/water solvent mixture gave **P6**,[86] which was deprotected with 10% Pd/C under H_2 in ethyl acetate to give **P7**.[87] Imide

condensation between **P7** and **P1** in molten imidazole afforded **3**.[15] Further, **P5** was reacted with 4-aminophenylboronic acid pinacol ester and 4-aminobiphenyl-4′-boronic acid pinacol ester using Suzuki−Miyaura cross-coupling conditions to afford **P8** and **P9**, respectively.[69] Deprotection using the previously described reductive conditions to give **P10** and **P11**[69] followed by imide condensations with **P1** yielded **4** and **5**, respectively.[15]

Compound **2** was present as a mixture of isomers that could be distinguished by ^{1}H NMR spectroscopy using the resonances of the 9-methyl and *tert*-butyl protons on the Xan bridge. In **2A** (Figure 1), the two methyl groups experience different magnetic environments, while in **2B**, the two methyl groups experience the same magnetic environment. The ^{1}H NMR resonances in $CDCl_3$ at 25 °C reflect both of these structures with two singlets of equal intensity (3H) at 1.92 and 1.81 ppm (**2A**) and another more intense (6H) singlet at 1.90 ppm (**2B**) (Figure S1A in the SI). In $CDCl_3$, two of these singlets overlap with the multiplet from the two protons on the tertiary carbons of the 2-ethylhexyl groups, but the ratio of nonequivalent to equivalent methyl protons in toluene-d_8 indicates a **2A**:**2B** ratio of ∼9:10 (Figure S1B). Similarly, two *tert*-butyl proton resonances from the two isomers are evident at around 1.34 ppm. Variable-temperature ^{1}H NMR measurements up to 100 °C failed to interconvert the two isomers (Figure S1C), and all attempts to isolate the two isomer bands by HPLC yielded mixtures of isomers.

X-ray Crystallography. Dimer **1** crystallizes in the monoclinic crystal system in the $P2_1/c$ space group with one molecule in the asymmetric unit and a total of four molecules in the unit cell (Tables S3 and S4 in the SI). The unit cell parameters are a = 23.3440 Å, b = 13.6417 Å, c = 15.9048 Å, and β = 105.030°. The compound crystallizes with a total of four molecules of chloroform and four molecules of methanol in the unit cell. The two PMI subunits adopt a ∼70° angle geometry relative to the Xan (φ in Figure 2) to adopt a shorter $\pi−\pi$ distance of 3.3 Å between PMIs. Dimer **5** crystallizes in the triclinic crystal system in the $P\bar{1}$ space group with two molecules in the asymmetric unit and a total of four molecules in the unit cell (Tables S5 and S6). The unit cell parameters are a = 17.3715 Å, b = 21.0110 Å, c = 21.0234 Å, α = 73.849°, β = 105.030°, and γ = 69.341°. The dimer structure has another dimer intercalated, forming a strong association between the PMIs of separate dimers. As a result, there is a distortion between the PMIs within each dimer, resulting in a ψ angle of 26° and a larger $\pi−\pi$ distance of 6.8 Å. The two crystal structures are summarized in Figure 2, and pictures of the structures are shown in Figure 3.

Molecular Modeling. Structures computed using DFT along with a polarizable continuum model for the solvent as described in the Experimental Section were used to determine the relative orientations of the PMIs with respect to each other and the Xan bridge in CH_2Cl_2 (Tables S7−S12). Relevant angles and distances are summarized in Figure 2, and pictures of the structures are shown in Figures 3 and S19. The angle θ is defined as the angle between the transition dipole moment for the $S_1 \leftarrow S_0$ transition (in-plane with the long axis of PMI) and a line connecting the geometric centers of the molecules, in keeping with Kasha et al.[88] The calculations showed that $\theta_{avg} \geq$ 66° for **1−3** and θ_{avg} = 54° and 34° for **4** and **5**, respectively. The large difference between θ_1 and θ_2 for **5** indicates that the PMIs are tilted toward each other in that direction, while the large ψ values for every molecule except **2B** indicate a tilt between the long axes of the PMIs in the perpendicular

14915

dx.doi.org/10.1021/ja507653p | *J. Am. Chem. Soc.* 2014, 136, 14912−14923
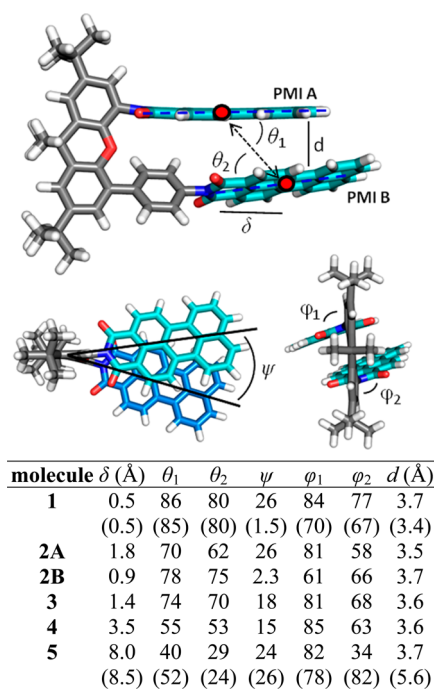
Figure 2. Schematic detailing the geometric parameters of covalent PMI dimers. The structures of **1** and **4** are shown. PMI A is defined as the PMI attached directly to the Xan backbone through the imide, except for **2A** and **2B**, where the PMIs are identical and have no imide attachment. δ is the distance between the PMI centers of mass (red dots) along the long axis of PMI; θ is the angle between the transition dipole moment (along the direction of the blue dotted line) and the vector between the centers of mass; ψ is the rotational displacement angle; φ is the dihedral angle between PMI and Xan; and d is the smallest atom-to-atom distance between the PMIs. All angles are reported in degrees. The reported values are for the computed structures, except for the values in parentheses, which are from the crystal structures.

molecule	δ (Å)	θ_1	θ_2	ψ	φ_1	φ_2	d (Å)
1	0.5	86	80	26	84	77	3.7
	(0.5)	(85)	(80)	(1.5)	(70)	(67)	(3.4)
2A	1.8	70	62	26	81	58	3.5
2B	0.9	78	75	2.3	61	66	3.7
3	1.4	74	70	18	81	68	3.6
4	3.5	55	53	15	85	63	3.6
5	8.0	40	29	24	82	34	3.7
	(8.5)	(52)	(24)	(26)	(78)	(82)	(5.6)

direction. Values of φ, the dihedral angle between the plane of the PMI π system and that of the Xan bridge, were obtained by computing the angle using four atoms: the oxygen on the Xan bridge, the Xan 4- or 5-carbon attached directly to the PMI or the phenyl spacer, the PMI atom attached to the Xan bridge or phenyl spacer (imide nitrogen or carbon at the 9-position), and a nearby atom (the carbonyl oxygen or the carbon at the 10-position). The difference between the two dihedral angles in **2A** indicates that the Xan bridge is bent, not that the PMIs are not parallel. The calculated dihedral angles suggest that there is the most $\pi-\pi$ overlap with the PMIs closest to parallel in **2B**, while

the PMIs are farthest from parallel in **5**. The distance between the 4- and 5-positions on the Xan bridge is 4.7 Å, but the PMIs tilt toward each other in the θ and φ directions to achieve a $\pi-\pi$ stacking distance (d) of ~3.6 Å at the closest points.

The X-ray structures and computed structures for **1** and **5** are compared in Figures 2 and 3. Each of the crystal structures yields nearly identical φ_1 and φ_2 compared with the much larger difference in the computed geometries. The crystal structure for **1** shows PMIs that are nearly parallel to each other in both the θ and the ψ directions, which is again not true for the computed geometries. Additionally, the intercalated crystal structure of **5** has a unique bent Xan backbone. Because of these significant differences, the crystal structures are assumed to be poor approximations of the molecular geometries in solution, and the computed solution structures are used in the analysis.

Steady-State Optical Spectroscopy. The normalized steady-state absorption and emission spectra of **1**−**5** and **PMI** in CH_2Cl_2 are provided in Figures 4 and 5, and the spectral properties are summarized in Table 1. **PMI** has an absorption maximum at 481 nm (Figure 4A) that is assigned to the (0,1) transition and a lower-energy vibronic band of nearly equal intensity at 503 nm that corresponds to the (0,0) transition. Cofacial $\pi-\pi$ stacking of PMI in **1** results in a more intense (0,1) absorption band at 476 nm relative to the redder band, which is red-shifted to 518 nm. For the cofacially stacked PMIs in **2** and **3**, a similar though smaller intensity difference is also observed at 485 and 478 nm compared with the red-shifted bands at 531 and 522 nm, respectively. When a phenyl spacer is inserted between the Xan bridge and one of the PMIs in **4**, the changes in the (0,1) band intensity at 483 nm relative to the red-shifted band at 515 nm are small (Figure 5A). Dimer **5** with a biphenyl spacer demonstrates a marked difference from any of the other compounds, with a dominant (0,0) band at 511 nm compared with the (0,1) band at 488 nm.

The steady-state emission spectrum of **PMI** displays a vibronic progression with a maximum at 541 nm [the (0,0) transition], a smaller peak at 578 nm, and a slight shoulder at 640 nm; the fluorescence quantum yield (Φ_F) is 0.96 (Figure 4B).[17] In contrast, the fluorescence from cofacial π-stacked dimers **1**−**3** is highly quenched. The spectra are characterized by the appearance of broad, featureless emission bands with large Stokes shifts, and the mixture of **2A** and **2B** produces a particularly broad emission spectrum. The vibronic structure on the blue edge of the emission spectrum of **1** is attributed to a minor monomeric impurity (~0.1%). Compound **3** has a somewhat higher fluorescence quantum yield ($\Phi_F = 0.11$) than do **1** and **2** ($\Phi_F = 0.02$ and 0.03, respectively). As with the
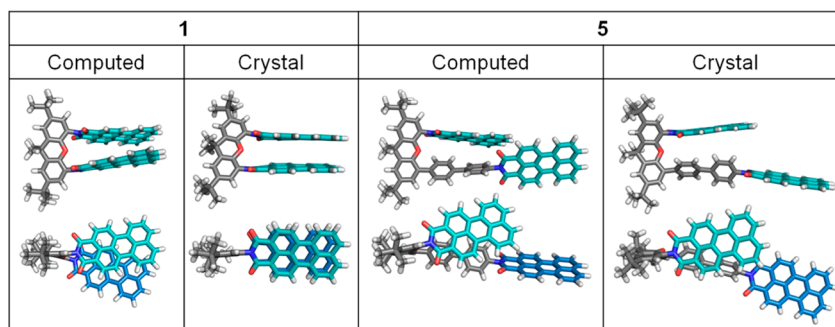
Figure 3. DFT-computed ground-state structures and crystal structures for **1** and **5**.
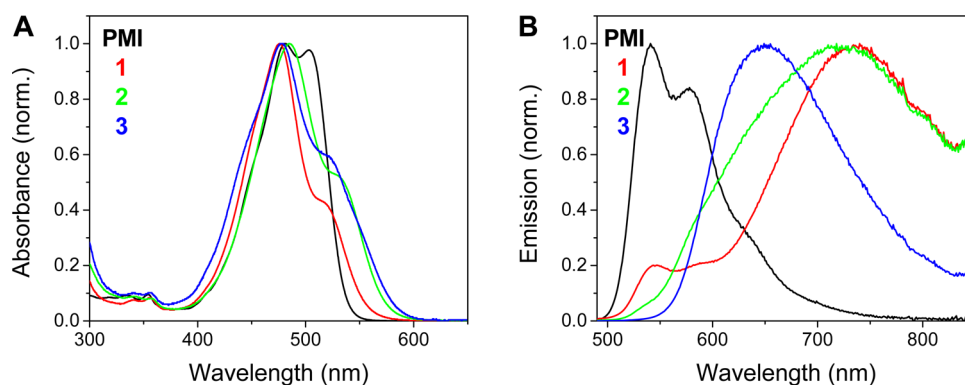
Figure 4. Normalized (A) absorption spectra and (B) emission spectra with excitation at 470 nm of **1** (red), **2** (green), and **3** (blue) compared with **PMI** (black) in CH_2Cl_2.
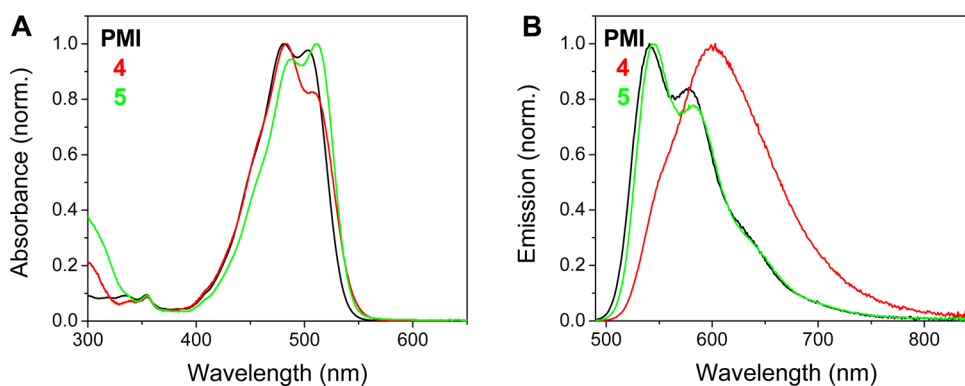
Figure 5. Normalized (A) absorption spectra and (B) emission spectra with excitation at 470 nm of **4** (red) and **5** (green) compared with **PMI** (black) in CH_2Cl_2.

Table 1. Steady-State Spectral Data

molecule	λ_{max}^{abs} (nm)	λ_{max}^{em} (nm)	λ_{max}^{em} (eV)	Φ_F
PMI	481	541	2.29	0.96
1	476	740	1.68	0.02
2	485	718	1.73	0.03
3	478	649	1.91	0.11
4	483	603	2.06	0.61
5	511	543	2.28	0.92

Table 2. Time-Resolved Kinetics

molecule	fsTA		TRF
	τ_{exc} (ps)	τ_{rlx} (ps)	τ_F (ns)
PMI	–	1.5 ± 0.6^a	5.26 ± 0.03
1	1.0 ± 0.1	17 ± 5	6.90 ± 0.03
2	1.0 ± 0.1	12 ± 1	7.93 ± 0.05
3	1.1 ± 0.5	9 ± 2	11.43 ± 0.06
4	1.3 ± 0.3	8 ± 3	12.81 ± 0.06
5	–	2 ± 1	4.76 ± 0.04

^{a}Vibrational cooling of the ^{1}***PMI** monomer.

absorption spectra, the emission spectra of molecules **4** and **5** are quite similar to that of monomeric **PMI** (Figure 5B), though the fluorescence spectrum of **4** is slightly broadened and red-shifted relative to that of **PMI** with a shoulder on the blue edge. Dimers **4** and **5** show slightly quenched emission relative to **PMI** with $\Phi_F = 0.61$ and 0.92, respectively.

Time-Resolved Optical Spectroscopy. Picosecond TRF spectra and kinetic traces at the emission maxima in CH_2Cl_2 are shown in Figures S2–S7 for **PMI** and **1**–**5**. The fluorescence lifetime of the **PMI** monomer is $\tau_F = 5.26 \pm 0.03$ ns, while the lifetimes of molecules **1** ($\tau_F = 6.90 \pm 0.03$ ns) through **4** ($\tau_F = 12.81 \pm 0.06$ ns) increase as the structures deviate from the maximally overlapped cofacial structure. Conversely, the fluorescence lifetime of **5** decreases slightly ($\tau_F = 4.76 \pm 0.04$ ns) relative to that of **PMI**. The fluorescence lifetimes are summarized in Table 2.

The visible and NIR fsTA spectra of **PMI** in CH_2Cl_2 following 100 fs excitation at 490 nm are shown in Figure 6A. The data from the separate visible and NIR experiments are corrected for GDD and t_0, but the relative magnitudes of ΔA

between the two experiments are not quantitatively scaled. Photoexcitation of **PMI** results in a ground-state bleach at 430–560 nm, which is accompanied by a very small stimulated-emission feature at 668–744 nm, a transient absorption feature corresponding to ^{1}***PMI** at 611 nm with a much smaller band at 850–1200 nm, and a small absorption tail extending to 1600 nm. SVD and global analysis of the combined visible and NIR three-dimensional data set (ΔA vs time and wavelength) yielded the decay-associated spectra presented in Figure S8 and the lifetimes summarized in Table 2. The main ^{1}***PMI** absorption exhibits a maximum at 620 nm immediately after excitation, which blue-shifts to 611 nm in $\tau_{rlx} = 1.5 \pm 0.6$ ps. The maximum of the weaker absorption shifts from 1073 to 1056 nm on the same time scale.

Additional features and a lack of stimulated emission are observed for the cofacial dimers **1**–**3** and the phenyl-spaced dimer **4** (Figure 6). Biexponential evolution of the visible spectra for **1** occurs with $\tau_{exc} = 1.0 \pm 0.1$ ps and $\tau_{rlx} = 17 \pm 5$ ps
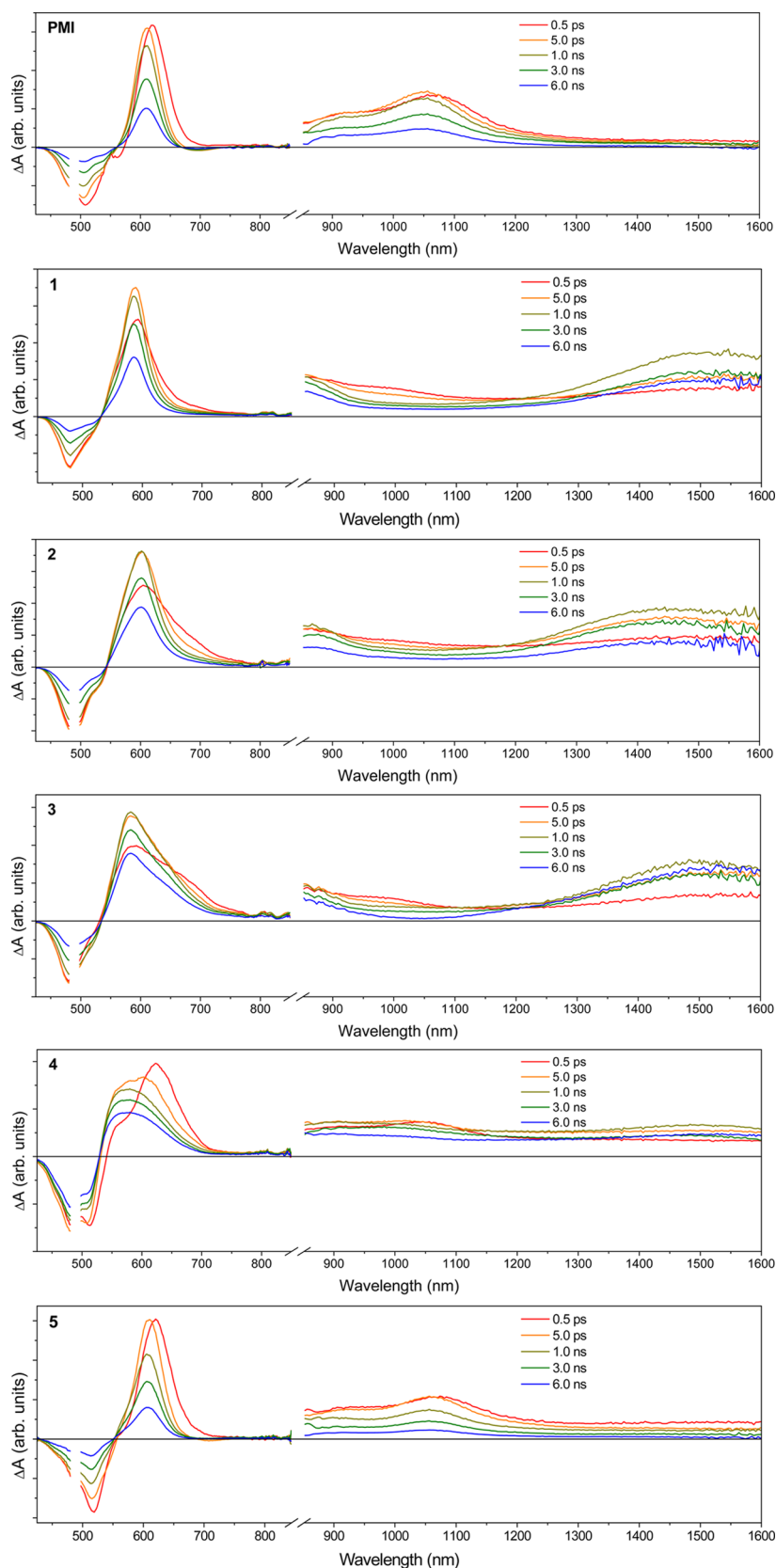
Figure 6. Femtosecond transient absorption spectra of PMI and **1−5** in CH$_2$Cl$_2$ following excitation with a 490 nm laser pulse.

as the main transient absorption feature sharpens and blue-shifts (Figure S8). In the NIR, the feature at 1000 nm decays and a new broad absorption appears with the same two time constants. This feature can be fit to a Gaussian line shape

function with $\lambda_{max} = 1514 \pm 1$ nm (0.82 eV) (Figure S10 and Table 3). Time constants for the blue shift of the visible band and the growth of the NIR transition for **1−4** are given in Table 2. The main long-lived transient absorption features in the

Table 3. Gaussian Fits of the NIR Feature in the fsTA Spectra[a]

molecule	λ_{max} (nm)	λ_{max} (eV)	fwhm (eV)
1	1514 ± 1	0.82	0.19
2	1457 ± 2	0.85	0.23
3	1510 ± 2	0.82	0.19
4	1485 ± 2	0.83	0.11

[a]Standard errors of the Gaussian fits are all <1 meV.

visible spectra are broader for **2−4** than for **1** or monomeric **PMI**, and the blue shifts are more pronounced. The two isomers of **2** show a broad NIR feature at 1457 ± 2 nm, while **3** shows a maximum identical to that of **1** at 1510 ± 2 nm. In contrast to **1−3**, the visible transient absorption feature of compound **4** evolves into a very broad band that lacks a sharp maximum with accompanying growth of only a weak NIR feature at 1485 ± 2 nm (Figures 6 and S9). Gaussian fits are shown in Figures S11−S13 and summarized in Table 3. There is a small residual transient absorption for **1−3** at 475−520 nm resembling that of [3]*PMI in the nsTA spectra (Figures S14−S16) that is not present for **4** or **5** (Figures S17 and S18).[27] The time constants for these decays are too close to the 7 ns instrument response to be determined accurately. The biphenyl-spaced PMIs of **5** behave almost identically to monomeric **PMI** with a small stimulated emission feature at 688−745 nm, a blue-shift of the main transient absorption band in τ_{rlx} = 2 ± 1 ps, and a slightly shorter τ_F of 4.76 ± 0.04 ns for fluorescence decay (Figures 6 and S9).

■ DISCUSSION

Steady-State Absorption and Emission Spectroscopy. When chromophores with strongly coupled transition dipole moments adopt a cofacial arrangement (H-aggregate regime, $54.7° < \theta \leq 90°$; Figure 2), the excited state of the system splits into two exciton states for which the electronic transition between the ground and upper exciton state is symmetry-allowed, resulting in an overall blue shift in the absorption spectrum (Figure 7).[88] When the transition dipoles of the
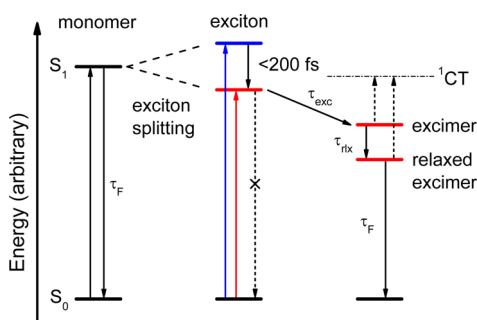
Figure 7. Schematic detailing the relative energy levels and photophysical processes for molecules **1−5**.

chromophores are offset along their long axes (J-aggregate regime, $0° \leq \theta < 54.7°$; Figure 2), the electronic transition between the ground state and the lower-energy exciton state is allowed, which results in an apparent red shift in the absorption spectrum. On the basis of this zeroth-order molecular exciton model, H-aggregate (**1−3**) and J-aggregate (**4−5**) behavior is expected from the PMI dimer series studied here. Indeed, the observed steady-state absorption spectra for **1−3** display blue-

shifted (0,0) transitions that overlap strongly with the (0,1) transitions and increase the absorption at that wavelength, consistent with H-aggregate behavior. Extensions to the exciton model that incorporate vibronic coupling relax the selection rules for transitions between the ground state and the exciton states and allow the lowest-energy observed transition to be assigned to the partially allowed (0,0) transition to the lower-energy exciton state.[89] In addition, transition density models show that the "magic angle" criterion used to differentiate H- from J-type aggregates is not always accurate.[90−97] Molecule **1** has the largest intensity ratio of the high-energy allowed to low-energy forbidden exciton transitions, which indicates stronger electronic coupling than in either **2** or **3**.

The broad, featureless, red-shifted emission spectra observed for **1−3** suggest that an excimer state in which the PMIs are electronically coupled in the excited state is formed from the initial excitonic state. The excimer emission energy reflects the energy gap between the vibrationally relaxed excimer state and the ground state of the molecule in the same conformation. It is well-established that the energy of this transition depends on both conformational relaxation and electronic coupling within the dimer.[70] Structural changes that stabilize the excimer conversely serve to destabilize the ground state and thus decrease the energy of the emission. The excimer is stabilized by mixing of the two locally excited Frenkel (exciton) states, derived from the configurations ^{1}*PMI_A−PMI_B and PMI_A−^{1}*PMI_B, with the charge transfer (CT) configurations PMI_A^-−PMI_2^+ and PMI_A^+−PMI_B^- to produce four states of mixed Frenkel−CT character.[98] Molecule **1** has the lowest excimer emission energy of the series, which indicates that it has the strongest coupling between the PMI molecules. This correlates well with the steady-state absorption experiments, which show that **1** has the largest exciton splitting as well. Additionally, **1** has the largest angle ψ of all the dimers (Figure 2) and thus requires a greater structural rearrangement to reach the relaxed excimer geometry, which is expected to have the long axes of the PMI molecules parallel to one another.[98] However, in the ground state, this relaxed geometry is energetically higher, which decreases the emission energy somewhat. The additional breadth of the emission spectrum for **2** is consistent with the presence of the two isomers **2A** and **2B**, as they have differing degrees of coupling and stabilization of their relaxed excimer states. On the basis of the energy-minimized structures of **2A** and **2B**, we expect a lower-energy emission band for **2B**, which has a smaller $\pi-\pi$ stacking distance and more direct overlap between the π systems. The average quantum yield for the isomer mixture, $\Phi_F = 0.03$, is reported because the individual quantum yields for the two isomers could not be obtained. However, the ^{1}H NMR spectrum of the mixture shows that **2A** and **2B** are present in almost equal amounts, so both isomers must have very low fluorescence quantum yields. Consistent with the steady-state absorption spectra, the higher fluorescence quantum yield for the excimer of **3** ($\Phi_F = 0.11$) compared with **1** ($\Phi_F = 0.02$) and **2** demonstrates that the PMI−PMI coupling is the weakest for **3** and that the nonradiative decay typical of strongly coupled H-aggregates is less dominant.[70]

The energy-minimized structures of **4** and **5** show that both should behave as J-aggregates, with $\theta_{avg} = 54°$ and $34°$, respectively.[88] Both exhibit a small red shift of the (0,0) absorption band, and the band is slightly enhanced for **5**, as expected for a J-aggregate. However, molecule **4** shows a more intense (0,1) band similar to those of H-aggregates **1−3**, which

indicates that the electronic coupling between the PMI molecules in **4** is still significant.[69,71] The emission spectrum of **4** demonstrates that excimer formation occurs, but the Frenkel−CT exciton mixing is weaker than that in **1**−**3** because the excimer emission energy is higher, and there is a shoulder on the blue edge of the spectrum resulting from emission from the precursor lower exciton state, which is expected of J-aggregates.[99] Molecule **5** does not form an excimer and does not have significantly quenched fluorescence, primarily because of the long distance $\delta = 8.0$ Å and the difference in φ between the PMI molecules, which diminishes the electronic coupling between them.

Time-Resolved Dynamics. The picosecond TRF measurements yielded fluorescence lifetimes ranging from 4.76 to 12.81 ns for **1**−**5**, compared with $\tau_F = 5.26 \pm 0.03$ ns for [1]*PMI. The extended lifetimes and red-shifted emission for **1**−**4** suggest that in each case emission occurs from an excimer state (Figure 7). The shortest fluorescence lifetime is observed for **1** and can be explained by either increased vibrational interactions due to the proximity and electronic coupling of the PMIs or by enhanced internal conversion due to the lower energy gap (energy gap law), as discussed above.[100] Increasing the offset between the PMIs along their short and long axes results in an increase in the excimer-state lifetime from $\tau_F = 6.90 \pm 0.03$ ns for **1** to 12.81 ± 0.06 ns for **4**. As expected,[101] these excimer lifetimes are not significantly different from those observed for extended PMI aggregates,[40] so the conclusions drawn here should apply to larger self-assembled aggregates and solid films of similar morphologies. Molecule **5** shows no evidence of excimer emission, so its fluorescence lifetime of 4.76 ± 0.04 ns, which is slightly shortened relative to that of **PMI**, may be attributed to additional vibronic coupling to the Xan bridge, which may increase the nonradiative decay rate.

Theoretical work on non-covalent PDI dimers by Schubert and co-workers[98,101] provides a framework with which the excimer formation dynamics in **1**−**4** observed by fsTA can be understood. Excitation to the upper Frenkel state is followed by internal conversion to the lower exciton state via a transiently populated CT state in ~200 fs, from which excimer formation occurs on a picosecond time scale. Such relaxation to the lower exciton state prior to excimer formation has previously been observed for PDI covalent dimers[59] and α-perylene crystals[102,103] by temperature-dependent and time-resolved fluorescence measurements.

Two features in the fsTA spectra allow us to follow the formation of the excimer for **1**−**4**. Stimulated emission of the analogous PDI dimers lasts for only ~200 fs before internal conversion from the upper to the lower Frenkel state and subsequent excimer formation in τ_{exc} occurs (Figure 7).[98] If PMI excimer formation follows a similar pathway, we would not expect to observe any stimulated emission because of the time resolution of our experiment. Indeed, dimers **1**−**4** show no stimulated emission, while **5** displays a small amount at early times. Thus, the early fsTA spectra for **1**−**4** are assigned to formation of the excimer state from the lower Frenkel state. In the series **1** to **4**, the visible fsTA spectra become increasingly broadened, which likely results from the increasing electronic inequivalence of the two PMI chromophores due to their different connectivity to the Xan bridge. Population of the excimer state is observed as a blue shift and sharpening of the S_1 absorption spectrum, as has been observed previously by us for self-assembled PMI excimers.[40] Within the molecules investigated here, the time scale of excimer formation from

the lower exciton state is independent of the conformation as long as the coupling is sufficient for the process to occur, as the time constants for all four molecules are $\tau_{exc} \approx 1$ ps. It is important to note that this process is distinct from the observed blue shift of the monomeric [1]*PMI spectrum, which is most likely due to vibrational relaxation. In support of this conclusion, the NIR band near 1450−1500 nm begins to rise with the same time constant and is similar to bands observed previously for cofacial covalent PDI excimers.[70,71,73] It is assigned to the transition from the lowest PMI excimer state to a PMI$^+$−PMI$^-$ singlet charge transfer ([1]CT) state (Figure 7).

The second component in the biexponential kinetics of **1**−**4** is $\tau_{rlx} = 8$−17 ps, which can be assigned to geometric rearrangement from the initial unrelaxed excimer state to a more relaxed excimer conformation (Figure 7).[1,70,71] The blue shifts in the NIR features accompanying these rises support this assignment. Relaxation to a lower-energy excimer state would necessarily raise the energy of the transition to the [1]CT states. The decreasing time constants for structural rearrangement in going from **1** to **4** are consistent with the TRF data and support the idea that steric hindrance to that motion is decreasing in the series **1** to **4**. The long decay time constant observed for **1** is also consistent with the larger rotation in ψ required to reach the relaxed excimer state, as discussed above. Thus, the decreasing electronic coupling in the order **1** > **2** > **3** > **4** corresponds to an increasing ability of the PMIs to rearrange to longer-lived excimer states.

Comparison to PDI Dimers. A comparison of the excimer formation and decay lifetimes for **1**−**4** and the lack of excimer formation in **5** reveal similar trends for PMI as for PDI. A cofacial Xan-bridged PDI molecule that corresponds to **1** has excimer formation time constants in toluene of $\tau_{exc} = 1.8 \pm 0.7$ ps and $\tau_{rlx} = 14 \pm 4$ ps, which are within the experimental error of the excimer formation times of $\tau_{exc} = 1.0 \pm 0.1$ ps and $\tau_{rlx} = 17 \pm 5$ ps observed for **1**.[70] The similarity in τ_{exc} is not surprising given the comparable chromophore orientations. The agreement in τ_{rlx} is consistent with its assignment to structural rearrangement and the identical connectivity of the Xan bridge to PMI in **1** and to PDI in the corresponding dimer.

We have also studied a pair of triptycene-bridged PDI dimers analogous to **1** and **4**, which eliminates the oxidation of Xan by [1]*PDI that competes with excimer formation in the slip-stacked Xan-bridged PDI dimer analogous to **4**.[71] Photoexcitation of the triptycene-bridged cofacial PDI dimer forms the initial excimer state in $\tau_{exc} = 2.2 \pm 0.2$ ps in CH_2Cl_2, which subsequently relaxes in $\tau_{rlx} = 24 \pm 6$ ps, while the triptycene-bridged slip-stacked PDI dimer forms the excimer state in $\tau_{exc} = 12 \pm 3$ ps with no readily observable distinction between the initial excimer formation and its conformational relaxation. Excimer formation in the triptycene-bridged slip-stacked PDI dimer may be slowed by steric interference of the PDI alkyl tails that preclude optimal π−π stacking, so the excimer state relaxes at a rate comparable to that at which it initially forms. Dimers **1** and **4** do not have the alkyl tails that the analogous PDI dimers have, so their PMI π systems can approach more closely. The lifetimes of the relaxed excimer states of **1** and **4** are $\tau_F = 6.90 \pm 0.03$ and 12.81 ± 0.06 ns, while those of the corresponding triptycene-bridged PDI dimers are $\tau_F = 12.0 \pm 0.3$ and 24.1 ± 0.4 ns, respectively.[71] The shorter excimer-state lifetimes of **1** and **4** may result from stronger electronic coupling of the PMI molecules relative to that of the PDI molecules, once again as a result of better π overlap in the PMI dimers relative to the PDI

dimers. Analogous to PDI,[69] the biphenyl spacer between the cofacial PMI molecules in **5** prevents excimer formation.

The NIR transition energies (E_{NIR}) from the lowest $^{1*}(PMI-PMI)$ states to the $^{1}(PMI^{+}-PMI^{-})$ ^{1}CT states provide an additional metric for comparing the excimer states of the PMI dimers with those of the corresponding PDI dimers. For example, comparison of the cofacial and slip-stacked PMI dimers shows that the NIR transition energies for **1** (0.82 eV) and **4** (0.83 eV) are nearly identical. Changes in E_{NIR} can be attributed to changes in the stability of the excimer state and/or the ^{1}CT state. Since the excimer-state energies (E_{XMR}) of **1** and **4** are 1.68 and 2.06 eV, respectively, the fact that E_{NIR} is similar for these two molecules implies that the energies of the ^{1}CT states (E_{CT}) differ by a comparable amount. E_{CT} can be estimated as $E_{CT} = E_{XMR} + E_{NIR}$.[70] In this case, $E_{CT} = 2.50$ and 2.89 eV for **1** and **4**, respectively. In comparison, for the corresponding cofacial and slip-stacked triptycene-bridged PDI dimers, $E_{NIR} = 0.74$ and 0.87 eV, respectively, and $E_{XMR} = 1.67$ and 1.92 eV, respectively, giving $E_{CT} = 2.41$ and 2.79 eV, respectively.[71] These data suggest that cofacial $\pi-\pi$ stacking provides a similar significant degree of stabilization of the ^{1}CT state for both PMI and PDI dimers relative to slip-stacking.

Triplet State Formation. The excimer states of **1–3** decay predominantly to the ground state with only low yields of $^{3*}PMI$, which most likely results from spin–orbit-induced intersystem crossing (SO-ISC). Previous studies of cofacial Xan-bridged PDI molecules found that SO-ISC for $^{1*}(PDI)_2$ in CH_2Cl_2 occurs in ~23 ns.[61] In that case, the triplet quantum yields were estimated to be near 50% with competing excimer decay to the ground state in 18 ns. The low triplet yield for the PMI dimers can be explained by the relatively short excimer lifetime, which kinetically outcompetes SO-ISC within the excimer.

Alternatives to SO-ISC can be ruled out on the basis of energetic arguments. Charge separation resulting in either radical pair intersystem crossing[104–106] or spin–orbit charge-transfer intersystem crossing[107–110] are precluded as mechanisms for $^{3*}PMI$ formation because the free energies for charge separation to produce $Xan^{+\bullet}-PMI^{-\bullet}$ or $PMI^{+\bullet}-PMI^{-\bullet}$ from either $^{1*}PMI$ or $^{1*}(PMI)_2$ are very close to zero (Tables S1 and S2).[34,69] The data confirm this because charge separation and recombination would be expected to produce a sharp, blue-shifted absorption in a few picoseconds followed by recombination in ~1 ns.[36,69] Instead, the observed excited-state lifetimes are longer than that of the monomer, and the blue shifts are small. Additionally, $^{3*}PMI$ formation by singlet exciton fission is unlikely because the sum of the energies of two PMI triplet states is significantly higher than that of its vibrationally relaxed singlet state.[111]

CONCLUSIONS

We have investigated energy flow leading to excimer formation in a series of covalently bound PMI dimers using a xanthene bridge. The effects of connectivity, $\pi-\pi$ stacking offset, and chromophore orientation have been examined using steady-state and time-resolved optical spectroscopies. A comparison of the three cofacial PMI orientations in **1–3** demonstrates that the nearly cofacial geometry of **1** produces the strongest electronic coupling. Although the long-axis offset in **4** reduces the PMI–PMI electronic coupling, formation of the unrelaxed excimer still occurs in high yield, and this excimer has sufficient conformational flexibility to relax quickly to the longest-lived

excimer state. Significantly increasing the offset by using a biphenyl spacer to shift the PMI chromophores along their long molecular axis in **5** diminishes the coupling between the PMI chromophores enough to effectively prevent excimer formation. The PMI excimer is formed in dimers having conformations similar to those of the analogous PDI structures, which also exhibit fast excimer formation. However, PMI has the benefit of a much lower triplet yield due to competitive nonradiative decay of the excimer states. These factors may provide advantages for using PMI derivatives instead of PDI derivatives in assemblies for some energy and charge transport applications.

ASSOCIATED CONTENT

Ⓢ Supporting Information

Detailed synthesis and characterization of **P1–P3**, **P6–P7**, and **1–5**; additional TRF and fsTA results; nsTA results; an estimation of free energy changes for charge separation; crystallographic data for **1** and **5** (CIF); and DFT-computed ground state structures. This material is available free of charge via the Internet at http://pubs.acs.org.

AUTHOR INFORMATION

Corresponding Author
m-wasielewski@northwestern.edu

Author Contributions
†R.J.L. and K.M.L. contributed equally.

Notes
The authors declare no competing financial interest.

ACKNOWLEDGMENTS

REFERENCES

(1) Lim, J. M.; Kim, P.; Yoon, M.-C.; Sung, J.; Dehm, V.; Chen, Z.; Würthner, F.; Kim, D. *Chem. Sci.* **2013**, *4*, 388.
(2) Lehn, J.-M. *Science* **2002**, *295*, 2400.
(3) Luo, C.; Guldi, D. M.; Imahori, H.; Tamaki, K.; Sakata, Y. *J. Am. Chem. Soc.* **2000**, *122*, 6535.
(4) Wasielewski, M. R. *J. Org. Chem.* **2006**, *71*, 5051.
(5) Wasielewski, M. R. *Acc. Chem. Res.* **2009**, *42*, 1910.
(6) Weil, T.; Vosch, T.; Hofkens, J.; Peneva, K.; Müllen, K. *Angew. Chem., Int. Ed.* **2010**, *49*, 2.
(7) Le Pleux, L.; Smeigh, A. L.; Gibson, E.; Pellegrin, Y.; Blart, E.; Boschloo, G.; Hagfelt, A.; Hammarström, L.; Odobel, F. *Energy Environ. Sci.* **2011**, *4*, 2075.
(8) Marciniak, H.; Li, X.-Q.; Würthner, F.; Lochbrunner, S. *J. Phys. Chem. A* **2011**, *115*, 648.
(9) Ye, T.; Singh, R.; Butt, H.-J.; Floudas, G.; Keivanidis, P. E. *ACS Appl. Mater. Interfaces* **2013**, *5*, 11844.
(10) Chen, Z.; Stepanenko, V.; Dehm, V.; Prins, P.; Siebbeles, L. D. A.; Seibt, J.; Marquetand, P.; Engel, V.; Würthner, F. *Chem.—Eur. J.* **2007**, *13*, 436.
(11) Howard, I. A.; Laquai, F.; Keivanidis, P. E.; Friend, R. H.; Greenham, N. C. *J. Phys. Chem. C* **2009**, *113*, 21225.
(12) Walker, B. J.; Musser, A. J.; Beljonne, D.; Friend, R. H. *Nat. Chem.* **2013**, *5*, 1019.

(13) Beljonne, D.; Yamagata, H.; Brédas, J. L.; Spano, F. C.; Olivier, Y. *Phys. Rev. Lett.* **2013**, *110*, 226402.

(14) Eaton, S. W.; Shoer, L. E.; Karlen, S. D.; Dyar, S. M.; Margulies, E. A.; Veldkamp, B. S.; Ramanan, C.; Hartzler, D. A.; Savikhin, S.; Marks, T. J.; Wasielewski, M. R. *J. Am. Chem. Soc.* **2013**, *135*, 14701.

(15) Langhals, H. *Heterocycles* **1995**, *40*, 477.

(16) Feiler, L.; Langhals, H.; Polborn, K. *Liebigs Ann.* **1995**, 1229.

(17) Gosztola, D.; Niemczyk, M. P.; Svec, W.; Lukas, A. S.; Wasielewski, M. R. *J. Phys. Chem. A* **2000**, *104*, 6546.

(18) Herrmann, A.; Müllen, K. *Chem. Lett.* **2006**, *35*, 978.

(19) Li, C.; Schoneboom, J.; Liu, Z.; Pschierer, N. G.; Erk, P.; Herrmann, A.; Müllen, K. *Chem.—Eur. J.* **2009**, *15*, 878.

(20) Bullock, J. E.; Vagnini, M. T.; Ramanan, C.; Co, D. T.; Wilson, T. M.; Dicke, J. W.; Marks, T. J.; Wasielewski, M. R. *J. Phys. Chem. B* **2010**, *114*, 1794.

(21) Lefler, K. M.; Co, D. T.; Wasielewski, M. R. *J. Phys. Chem. Lett.* **2012**, *3*, 3798.

(22) Miller, S. E.; Schaller, R.; Mulloni, V.; Zhao, Y.; Just, E. M.; Johnson, R. C.; Wasielewski, M. R. *Chem. Phys.* **2002**, *275*, 167.

(23) Ahrens, M. J.; Fuller, M. J.; Wasielewski, M. R. *Chem. Mater.* **2003**, *15*, 2684.

(24) Cotlet, M.; Gronheid, R.; Habuchi, S.; Stefan, A.; Barbafina, A.; Müllen, K.; Hofkens, J.; De Schryver, F. C. *J. Am. Chem. Soc.* **2003**, *125*, 13609.

(25) Muthukumaran, K.; Loewe, R. S.; Kirmaier, C.; Hindin, E.; Schwartz, J. K.; Sazanovich, I. V.; Diers, J. R.; Bocian, D. F.; Holten, D.; Lindsey, J. S. *J. Phys. Chem. B* **2003**, *107*, 3431.

(26) Fuller, M. J.; Gusev, A. V.; Wasielewski, M. R. *Isr. J. Chem.* **2004**, *44*, 101.

(27) Hayes, R. T.; Walsh, C. J.; Wasielewski, M. R. *J. Phys. Chem. A* **2004**, *108*, 3253.

(28) Cotlet, M.; Vosch, T.; Habuchi, S.; Weil, T.; Müllen, K.; Hofkens, J.; De Schryver, F. *J. Am. Chem. Soc.* **2005**, *127*, 9760.

(29) Cremer, J.; Mena-Osteritz, E.; Pschierer, N. G.; Müllen, K.; Bäuerle, P. *Org. Biomol. Chem.* **2005**, *3*, 985.

(30) Bell, T. D. M.; Stefan, A.; Masuo, S.; Vosch, T.; Lor, M.; Cotlet, M.; Hofkens, J.; Bernhardt, S.; Müllen, K.; van der Auweraer, M.; Verhoeven, J. W.; De Schryver, F. C. *ChemPhysChem* **2005**, *6*, 942.

(31) Fron, E.; Lor, M.; Pilot, R.; Schweitzer, G.; Dincalp, H.; De Feyter, S.; Cremer, J.; Bäuerle, P.; Müllen, K.; Van der Auweraer, M.; De Schryver, F. C. *Photochem. Photobiol. Sci.* **2005**, *4*, 61.

(32) Fron, E.; Bell, T. D. M.; Van Vooren, A.; Schweitzer, G.; Cornil, J.; Beljonne, D.; Toele, P.; Jacob, J.; Müllen, K.; Hofkens, J.; Van der Auweraer, M.; De Schryver, F. C. *J. Am. Chem. Soc.* **2007**, *129*, 610.

(33) Melnikov, S. M.; Yeow, E. K. L.; Uji-I, H.; Cotlet, M.; Müllen, K.; De Schryver, F. C.; Enderlein, J.; Hofkens, J. *J. Phys. Chem. B* **2007**, *111*, 708.

(34) Veldman, D.; Chopin, S. M. A.; Meskers, S. C. J.; Janssen, R. A. J. *J. Phys. Chem. A* **2008**, *112*, 8617.

(35) Boixel, J.; Blart, E.; Pellegrin, Y.; Odobel, F.; Perin, N.; Chiorboli, C.; Fracasso, S.; Ravaglia, M.; Scandola, F. *Chem.—Eur. J.* **2010**, *16*, 9140.

(36) Vagnini, M. T.; Mara, M. W.; Harpham, M. R.; Huang, J.; Shelby, M. L.; Chen, L. X.; Wasielewski, M. R. *Chem. Sci.* **2013**, *4*, 3863.

(37) Warnan, J.; Gardner, J.; Le Pleux, L.; Petersson, J.; Pellegrin, Y.; Blart, E.; Hammarström, L.; Odobel, F. *J. Phys. Chem. C* **2014**, *118*, 103.

(38) Samorì, P.; Fechtenkötter, A.; Reuther, E.; Watson, M. D.; Severin, N.; Müllen, K.; Rabe, J. P. *Adv. Mater.* **2006**, *18*, 1317.

(39) Mativetsky, J. M.; Kastler, M.; Savage, R. C.; Gentilini, D.; Palma, M.; Pisula, W.; Müllen, K.; Samorì, P. *Adv. Funct. Mater.* **2009**, *19*, 2486.

(40) Lefler, K. M.; Kim, C. H.; Wu, Y.-L.; Wasielewski, M. R. *J. Phys. Chem. Lett.* **2014**, *5*, 1608.

(41) Ghosh, S.; Li, X.-Q.; Stepanenko, V.; Würthner, F. *Chem.—Eur. J.* **2008**, *14*, 11343.

(42) Kaiser, T. E.; Stepanenko, V.; Würthner, F. *J. Am. Chem. Soc.* **2009**, *131*, 6719.

(43) Bullock, J. E.; Carmieli, R.; Mickley, S. M.; Vura-Weis, J.; Wasielewski, M. R. *J. Am. Chem. Soc.* **2009**, *131*, 11919.

(44) Sinks, L. E.; Rybtchinski, B.; Iimura, M.; Jones, B. A.; Goshe, A. J.; Zuo, X.; Tiede, D. M.; Li, X.; Wasielewski, M. R. *Chem. Mater.* **2005**, *17*, 6295.

(45) Kelley, R. F.; Shin, W. S.; Rybtchinski, B.; Sinks, L. E.; Wasielewski, M. R. *J. Am. Chem. Soc.* **2007**, *129*, 3173.

(46) Ahrens, M. J.; Sinks, L. E.; Rybtchinski, B.; Liu, W.; Jones, B. A.; Giaimo, J. M.; Gusev, A. V.; Goshe, A. J.; Tiede, D. M.; Wasielewski, M. R. *J. Am. Chem. Soc.* **2004**, *126*, 8286.

(47) Li, X.; Sinks, L. E.; Rybtchinski, B.; Wasielewski, M. R. *J. Am. Chem. Soc.* **2004**, *126*, 10810.

(48) Rybtchinski, B.; Sinks, L. E.; Wasielewski, M. R. *J. Phys. Chem. A* **2004**, *108*, 7497.

(49) Rybtchinski, B.; Sinks, L. E.; Wasielewski, M. R. *J. Am. Chem. Soc.* **2004**, *126*, 12268.

(50) Ahrens, M. J.; Kelley, R. F.; Dance, Z. E. X.; Wasielewski, M. R. *Phys. Chem. Chem. Phys.* **2007**, *9*, 1469.

(51) Bullock, J. E.; Kelley, R. F.; Wasielewski, M. R. *PMSE Prepr.* **2007**, *96*, 805.

(52) Dossel, L. F.; Kamm, V.; Howard, I. A.; Laquai, F.; Pisula, W.; Feng, X.; Li, C.; Takase, M.; Kudernac, T.; De Feyter, S.; Müllen, K. *J. Am. Chem. Soc.* **2012**, *134*, 5876.

(53) Wang, W.; Li, L.-S.; Helms, G.; Zhou, H.-H.; Li, A. D. Q. *J. Am. Chem. Soc.* **2003**, *125*, 1120.

(54) Che, Y.; Datar, A.; Balakrishnan, K.; Zang, L. *J. Am. Chem. Soc.* **2007**, *129*, 7234.

(55) Dehm, V.; Chen, Z.; Baumeister, U.; Prins, P.; Siebbeles, L. D. A.; Würthner, F. *Org. Lett.* **2007**, *9*, 1085.

(56) Zhang, J.; Hoeben, F. J. M.; Pouderoijen, M. J.; Schenning, A. P. H. J.; Meijer, E. W.; De Schryver, F. C.; De Feyter, S. *Chem.—Eur. J.* **2006**, *12*, 9046.

(57) Würthner, F.; Thalacker, C.; Sautter, A. *Adv. Mater.* **1999**, *11*, 754.

(58) Schenning, A. P. H. J.; Herrikhuyzen, J. v.; Jonkheijm, P.; Chen, Z.; Würthner, F.; Meijer, E. W. *J. Am. Chem. Soc.* **2002**, *124*, 10252.

(59) Giaimo, J. M.; Lockard, J. V.; Sinks, L. E.; Scott, A. M.; Wilson, T. M.; Wasielewski, M. R. *J. Phys. Chem. A* **2008**, *112*, 2322.

(60) Yoo, H.; Bahng, H. W.; Wasielewski, M. R.; Kim, D. *Phys. Chem. Chem. Phys.* **2012**, *14*, 2001.

(61) Veldman, D.; Chopin, S. M. A.; Meskers, S. C. J.; Groeneveld, M. M.; Williams, R. M.; Janssen, R. A. J. *J. Phys. Chem. A* **2008**, *112*, 5846.

(62) Ambrosek, D.; Marciniak, H.; Lochbrunner, S.; Tatchen, J.; Li, X.-Q.; Würthner, F.; Kuhn, O. *Phys. Chem. Chem. Phys.* **2011**, *13*, 17649.

(63) Shao, C.; Grüne, M.; Stolte, M.; Würthner, F. *Chem.—Eur. J.* **2012**, *18*, 13665.

(64) Hippius, C.; van Stokkum, I. H. M.; Zangrando, E.; Williams, R. M.; Wykes, M.; Beljonne, D.; Würthner, F. *J. Phys. Chem. C* **2008**, *112*, 14626.

(65) Chen, Z.; Fimmel, B.; Würthner, F. *Org. Biomol. Chem.* **2012**, *10*, 5845.

(66) Tian, Y.; Stepanenko, V.; Kaiser, T. E.; Würthner, F.; Scheblynkin, I. G. *Nanoscale* **2012**, *4*, 218.

(67) Lin, H.; Camacho, R.; Tian, Y.; Kaiser, T. E.; Würthner, F.; Scheblynkin, I. G. *Nano Lett.* **2010**, *10*, 620.

(68) Kistler, K. A.; Pochas, C. M.; Yamagata, H.; Matsika, S.; Spano, F. C. *J. Phys. Chem. B* **2012**, *116*, 77.

(69) Lefler, K. M.; Brown, K. E.; Salamant, W. A.; Dyar, S. M.; Knowles, K. E.; Wasielewski, M. R. *J. Phys. Chem. A* **2013**, *117*, 10333.

(70) Brown, K. E.; Salamant, W. A.; Shoer, L. E.; Young, R. M.; Wasielewski, M. R. *J. Phys. Chem. Lett.* **2014**, *5*, 2588.

(71) Margulies, E. A.; Shoer, L. E.; Eaton, S. W.; Wasielewski, M. R. *Phys. Chem. Chem. Phys.* **2014**, DOI: 10.1039/C4CP03107E.

(72) Langhals, H.; Ismael, R. *Eur. J. Org. Chem.* **1998**, 1915.

(73) Katoh, R.; Katoh, E.; Nakashima, N.; Yuuki, M.; Kotani, M. *J. Phys. Chem. A* **1997**, *101*, 7725.

(74) Weil, T.; Reuther, E.; Beer, C.; Müllen, K. *Chem.—Eur. J.* **2004**, *10*, 1398.

(75) Gunderson, V. L.; Smeigh, A. L.; Kim, C. H.; Co, D. T.; Wasielewski, M. R. *J. Am. Chem. Soc.* **2012**, *134*, 4363.

(76) Young, R. M.; Dyar, S. M.; Barnes, J. C.; Juríček, M.; Stoddart, J. F.; Co, D. T.; Wasielewski, M. R. *J. Phys. Chem. A* **2013**, *117*, 12438.

(77) *Surface Xplorer*, version 2.2.3; Ultrafast Systems LLC: Sarasota, FL, 2010.

(78) Hanwell, M. D.; Curtis, D. E.; Lonie, D. C.; Vandermeersch, T.; Zurek, E.; Hutchison, G. R. *J. Cheminf.* **2012**, *4*, No. 17.

(79) Grimme, S.; Antony, J.; Ehrlich, S.; Krieg, H. *J. Chem. Phys.* **2010**, *132*, No. 154104.

(80) Shao, Y. *Phys. Chem. Chem. Phys.* **2006**, *8*, 3172.

(81) *PyMol*, version 1.2r1; Schrödinger, LLC: New York, 2010.

(82) Keerthi, A.; Liu, Y.; Wang, Q.; Valiyaveettil, S. *Chem.—Eur. J.* **2012**, *18*, 11669.

(83) Malaisé, G.; Barloy, L.; Osborn, J. A. *Tetrahedron Lett.* **2001**, *42*, 7417.

(84) Quante, H.; Müllen, K. *Angew. Chem., Int. Ed. Engl.* **1995**, *34*, 1323.

(85) Nolde, F.; Pisula, W.; Müller, S.; Kohl, C.; Müllen, K. *Chem. Mater.* **2006**, *18*, 3715.

(86) Dance, Z. E. X.; Ahrens, M. J.; Vega, A. M.; Butler-Ricks, A.; McCamant, D. W.; Ratner, M. A.; Wasielewski, M. R. *J. Am. Chem. Soc.* **2008**, *130*, 830.

(87) Kocieński, P. J. *Protecting Groups*, 3rd ed.; Georg Thieme Verlag: New York, 2005.

(88) Kasha, M.; Rawls, H. R.; El-Bayoumi, M. A. *Pure Appl. Chem.* **1965**, *11*, 371.

(89) Clark, A. E.; Qin, C.; Li, A. D. Q. *J. Am. Chem. Soc.* **2007**, *129*, 7586.

(90) Rosenoff, A. E.; Norland, K. S.; Ames, A. E.; Walworth, V. K.; Bird, G. R. *Photogr. Sci. Eng.* **1968**, *12*, 185.

(91) Czikkely, V.; Dreizler, G.; Forsterl, Hd; Kuhn, H.; Sonderma, J.; Tillmann, P.; Wiegand, J. *Z. Naturforsch., A: Astrophys., Phys. Phys. Chem.* **1969**, *24A*, 1821.

(92) Czikklely, V.; Forsterling, H. D.; Kuhn, H. *Chem. Phys. Lett.* **1970**, *6*, 207.

(93) Norland, K.; Ames, A.; Taylor, T. *Photogr. Sci. Eng.* **1970**, *14*, 295.

(94) Dietz, F.; Tyutyulk, N.; Passler, K. *J. Z. Chem.* **1972**, *12*, 145.

(95) Kuhn, H.; Kuhn, C. In *J-Aggregates*; Kobayashi, T., Ed.; World Scientific: Singapore, 1996; p 1.

(96) Millie, P.; Momicchioli, F.; Vanossi, D. *J. Phys. Chem. B* **2000**, *104*, 9621.

(97) Scholes, G. D.; Jordanides, X. J.; Fleming, G. R. *J. Phys. Chem. B* **2001**, *105*, 1640.

(98) Schubert, A.; Settels, V.; Liu, W.; Würthner, F.; Meier, C.; Fink, R. F.; Schindlbeck, S.; Lochbrunner, S.; Engels, B.; Engel, V. *J. Phys. Chem. Lett.* **2013**, *4*, 792.

(99) Würthner, F.; Kaiser, T. E.; Saha-Müller, C. R. *Angew. Chem., Int. Ed.* **2011**, *50*, 3376.

(100) Englman, R.; Jortner, J. *Mol. Phys.* **1970**, *18*, 145.

(101) Schubert, A.; Falge, M.; Kess, M.; Settels, V.; Lochbrunner, S.; Strunz, W. T.; Würthner, F.; Engels, B.; Engel, V. *J. Phys. Chem. A* **2014**, *118*, 1403.

(102) Walker, B.; Port, H.; Wolf, H. C. *Chem. Phys.* **1985**, *92*, 177.

(103) Ma, L.; Tan, K. J.; Jiang, H.; Kloc, C.; Michel-Beyerle, M.-E.; Gurzadyan, G. G. *J. Phys. Chem. A* **2014**, *118*, 838.

(104) Hore, P. J. In *Advanced EPR in Biology and Biochemistry*; Hoff, A. J., Ed.; Elsevier: Amsterdam, 1989; p 405.

(105) Buckley, C. D.; Hunter, D. A.; Hore, P. J.; McLauchlan, K. A. *Chem. Phys. Lett.* **1987**, *135*, 307.

(106) Closs, G. L.; Forbes, M. D. E.; Norris, J. R. *J. Phys. Chem.* **1987**, *91*, 3592.

(107) Okada, T.; Karaki, I.; Matsuzawa, E.; Mataga, N.; Sakata, Y.; Misumi, S. *J. Phys. Chem.* **1981**, *85*, 3957.

(108) van Willigan, H.; Jones, G., II; Farahat, M. S. *J. Phys. Chem.* **1996**, *100*, 3312.

(109) Dance, Z. E. X.; Mickley, S. M.; Wilson, T. M.; Ricks, A. B.; Scott, A. M.; Ratner, M. A.; Wasielewski, M. R. *J. Phys. Chem. A* **2008**, *112*, 4194.

(110) Dance, Z. E. X.; Mi, Q.; McCamant, D. W.; Ahrens, M. J.; Ratner, M. A.; Wasielewski, M. R. *J. Phys. Chem. B* **2006**, *110*, 25163.

(111) Smith, M. B.; Michl, J. *Chem. Rev.* **2010**, *110*, 6891.